Nanoscale

PAPER

View Article Online
View Journal | View Issue

Cite this: *Nanoscale*, 2024, **16**, 11109

Antimicrobial nanocomposite coatings for rapid intervention against catheter-associated urinary tract infections†‡

Dipanjana Patra,[a] Sreyan Ghosh,[b] Sudip Mukherjee,[b] Yash Acharya,[b] Riya Mukherjee[b] and Jayanta Haldar *[b,c]

Catheter-associated urinary tract infections (CAUTIs) pose a significant challenge in hospital settings. Current solutions available on the market involve incorporating antimicrobials and antiseptics into catheters. However, challenges such as uncontrolled release leading to undesirable toxicity, as well as the prevalence of antimicrobial resistance reduce the effectiveness of these solutions. Additionally, conventional antibiotics fail to effectively eradicate entrenched bacteria and metabolically suppressed bacteria present in the biofilm, necessitating the exploration of alternative strategies. Here, we introduce a novel polymer–nanocomposite coating that imparts rapid antimicrobial and anti-biofilm properties to coated urinary catheters. We have coated silicone-based urinary catheters with an organo-soluble antimicrobial polymer nanocomposite (APN), containing hydrophobic quaternized polyethyleneimine and zinc oxide nanoparticles, in a single step coating process. The coated surfaces exhibited rapid eradication of drug-resistant bacteria within 10–15 min, including *E. coli*, *K. pneumoniae*, MRSA, and *S. epidermidis*, as well as drug-resistant *C. albicans* fungi. APN coated catheters exhibited potent bactericidal activity against uropathogenic strains of *E. coli*, even when incubated in human urine. Furthermore, the stability of the coating and retention of antimicrobial activity was validated even after multiple washes. More importantly, this coating deterred biofilm formation on the catheter surface, and displayed rapid inactivation of metabolically repressed stationary phase and persister cells. The ability of the coated surfaces to disrupt bacterial membranes and induce the generation of intracellular reactive oxygen species (ROS) was assessed through different techniques, such as electron microscopy imaging, flow cytometry as well as fluorescence spectroscopy and microscopy. The surface coatings were found to be biocompatible in an *in vivo* mice model. Our simple one-step coating approach for catheters holds significant potential owing to its ability to tackle multidrug resistant bacteria and fungi, and the challenge of biofilm formation. This work brings us one step closer to enhancing patient care and safety in hospitals.

Received 15th February 2024,
Accepted 27th April 2024

DOI: 10.1039/d4nr00653d

rsc.li/nanoscale

Introduction

Urinary tract infections (UTIs) affect approximately 50% of women at some point in their lives leading to an overall annual cost of more than $1 billion.[1] One significant type of UTI is catheter-associated urinary tract infections (CAUTIs), with ~70–80% of complicated UTIs being attributed to indwelling catheters.[2–4] Close to one out of every five hospitalized patients undergoes catheterization during their hospital stay with catheters made of materials such as silicone, polyurethane rubber, *etc*.[5] The prolonged presence of a catheter within the urinary tract acts as a physiological as well as a mechanical irritant, and offers an easy substratum for the development of microbial biofilms, where bacteria or fungi can adhere to and colonize the catheter surface.[6] Coupled with the emergence of multidrug-resistant bacteria, the ability of

[a]*Chemistry and Physics of Materials Unit, Jawaharlal Nehru Centre for Advanced Scientific Research (JNCASR), Jakkur, Bengaluru-560064, Karnataka, India*
[b]*Antimicrobial Research Laboratory, New Chemistry Unit, Jawaharlal Nehru Centre for Advanced Scientific Research (JNCASR), Jakkur, Bengaluru-560064, Karnataka, India. E-mail: jayanta@jncasr.ac.in*
[c]*School of Advanced Materials, Jawaharlal Nehru Centre for Advanced Scientific Research (JNCASR), Jakkur, Bengaluru-560064, Karnataka, India*

†We dedicate this article to Professor Santanu Bhattacharya, in honour of his 65th birthday!

‡Electronic supplementary information (ESI) available: Materials and methods; detailed characterization; figures showing results of FT-IR analysis of ZnO nanoparticles, thermogravimetric analysis of QPEI-NHC_{16} and ZnO NP, scanning electron microscopy images of uncoated and coated silicone and catheter surfaces, scanning electron microscopy images of uncoated silicone surface and energy dispersive X-ray elemental analysis, stability of the coating after repeated washing of surfaces, antibacterial activity against different strains of Gram-positive and Gram-negative bacteria. See DOI: https://doi.org/10.1039/d4nr00653d

the most prevalent pathogens such as *E. coli*, MRSA and *Candida* to form biofilms on catheters has further complicated treatment options.[4,7] Bacteria within the biofilm are highly resistant to conventional drugs due to the impenetrable nature of the biofilm matrix and variable metabolic states of embedded cells, while also being less vulnerable to human immune cells compared to free-floating bacteria.[8–12]

Treating CAUTIs has become challenging, as higher doses of antibiotics are often required to eradicate the bacteria and clear the infection.[13–15] Even after robust antibiotic therapy, given the nature of infection and the persistence of invading bacterial and fungal pathogens, episodic recalcitrance of urinary tract infections is well reported.[16,17] Typically, catheters are replaced regularly to prevent infection, or patients are prescribed broad-spectrum antibiotics. However, both options are undesirable since they are tedious or may be ineffective against drug resistant bacteria, bringing further agony to the patient.[13,18] Untreated CAUTIs can lead to more severe conditions, including kidney infection (pyelonephritis) and potentially life-threating sepsis.[15,19–21] This underscores the need for a multi-pronged broad-spectrum bactericidal intervention for preventing and alleviating CAUTIs.

Current market practices involve impregnating catheters with antibiotics and antiseptics to decontaminate the local environment through their release; however, it can sometimes result in excessive leaching and reservoir exhaustion, reducing its effectiveness.[22,23] Additionally, the potential ineffectivity of current antibiotics against resistant strains is also a challenge. While there are some reports of antimicrobial coatings with broad-spectrum activity, very few studies have demonstrated the antimicrobial potential of coatings against catheter associated urinary tract infections.[24,25] Swift microbial adhesion and excessive biofilm formation in the case of CAUTIs necessitate rapid antimicrobial activity to mitigate and prevent catheter colonization.[26–28]

In this study, we aimed to address some of these challenges by developing a non-covalent antimicrobial polymer nanocomposite (APN) coating on silicone surfaces and urinary catheters, displaying a rapid microbicidal effect against drug-resistant bacteria and fungi, through multiple mechanisms of action. The coating was developed by the combination of two components, namely, a hydrophobic organosoluble polymer and zinc oxide nanoparticles. The rationale of choosing these two components lies in their individual properties. We chose a quaternized polyethyleneimine polymer (QPEI-NHC_{16}), which was reported to possess antibacterial properties. This polymer was engineered by quaternizing polyethyleneimine with a hexadecyl amide long chain.[29] Zinc oxide nanoparticles, which are known to possess antibacterial properties, were incorporated into the nanoformulation, along with the polymer.[30] The aim was to introduce synergy of antibacterial activity between the two components, and potentially obtain formulations with broad-spectrum activity. A physical mixture of the two components was dropcast onto silicone surfaces, which are a common catheter material. The coated surfaces were characterized using techniques including scanning electron microscopy (SEM) and atomic force microscopy (AFM). Our coating showed potent antibacterial properties against common catheter-associated pathogens, including *Escherichia coli*, *Enterococcal* strains, methicillin-resistant *Staphylococcus aureus* (MRSA), *Klebsiella pneumoniae*, and *Staphylococcus epidermidis* as well as antifungal activity against the fungal pathogen *Candida* spp. Biofilm inhibition studies were conducted against drug-resistant Gram-positive and Gram-negative bacteria. The retention of activity of the coating was checked after washing. The bactericidal activity of the coating was examined through spectroscopic methods. Furthermore, the biocompatibility of the APN-coated catheter was examined in an *in vivo* murine model through implantation.

Results and discussion

Synthesis and characterization

Synthesis and characterization of QPEI-NHC_{16}. The polymer, QPEI-NHC_{16}, was synthesized by quaternization of *N*-methyl PEI with *N*-hexadecyl-2-bromoethanamide.[29] Firstly, *N*-hexadecyl-2-bromoethanamide was obtained by reacting 1-amino hexadecane with bromoacetyl bromide. Next, *N*-methyl PEI was synthesized using the Eschweiler–Clarke methylation technique, employing commercially available branched polyethyleneimine (PEI, 750 kDa) (Fig. 1a). Finally, the *N*-methyl PEI was quaternized using *N*-hexadecyl-2-bromoethanamide, yielding QPEI-NHC_{16}. The polymer QPEI-NHC_{16} was characterized by FT-IR (Fig. 1b) and ^{1}H-NMR following previously established protocols.

Synthesis and characterization of ZnO nanoparticles. Zinc oxide nanoparticles were synthesized by reacting zinc acetylacetonate monohydrate with two surfactant moieties, oleyl amine and oleic acid, under inert conditions (Fig. 1c).[31] The high temperature process enables nucleation and the controlled growth of ZnO nanoparticles. The resulting nanoparticles were characterized by X-ray diffraction (XRD) analysis, which revealed distinct planes at (100), (002), (101), (102) (110), (103), (200) and (112) within the 30° to 80° range, confirming the formation of nanoparticles with a hexagonal closed packing (hcp) structure (Fig. 1d). The formation of nanoparticles was also confirmed by the observed Zn–O peak in the FT-IR spectrum at around 480 cm^{-1} (Fig. S1a‡). Transmission electron microscopy (TEM) was utilized to visualize the nanoparticles, where an average size of ~5.15 ± 0.93 nm was observed, with spherical morphology (Fig. 1e).

Thermal stability assessment. Thermal stability assessments were conducted on QPEI-NHC_{16} and the ZnO nanoparticles. QPEI-NHC_{16} showed robust thermal stability, manifesting weight loss or degradation only at 400 °C (Fig. S1b‡), which established its resilience as a thermally stable polymer. Because of the hydrophobic coating around the nanoparticle, stabilization over time was observed, up to a temperature of 650 °C (Fig. S1b‡).

Coating of surfaces and characterization. Antimicrobial polymer–nanocomposite (APN) solutions were prepared by

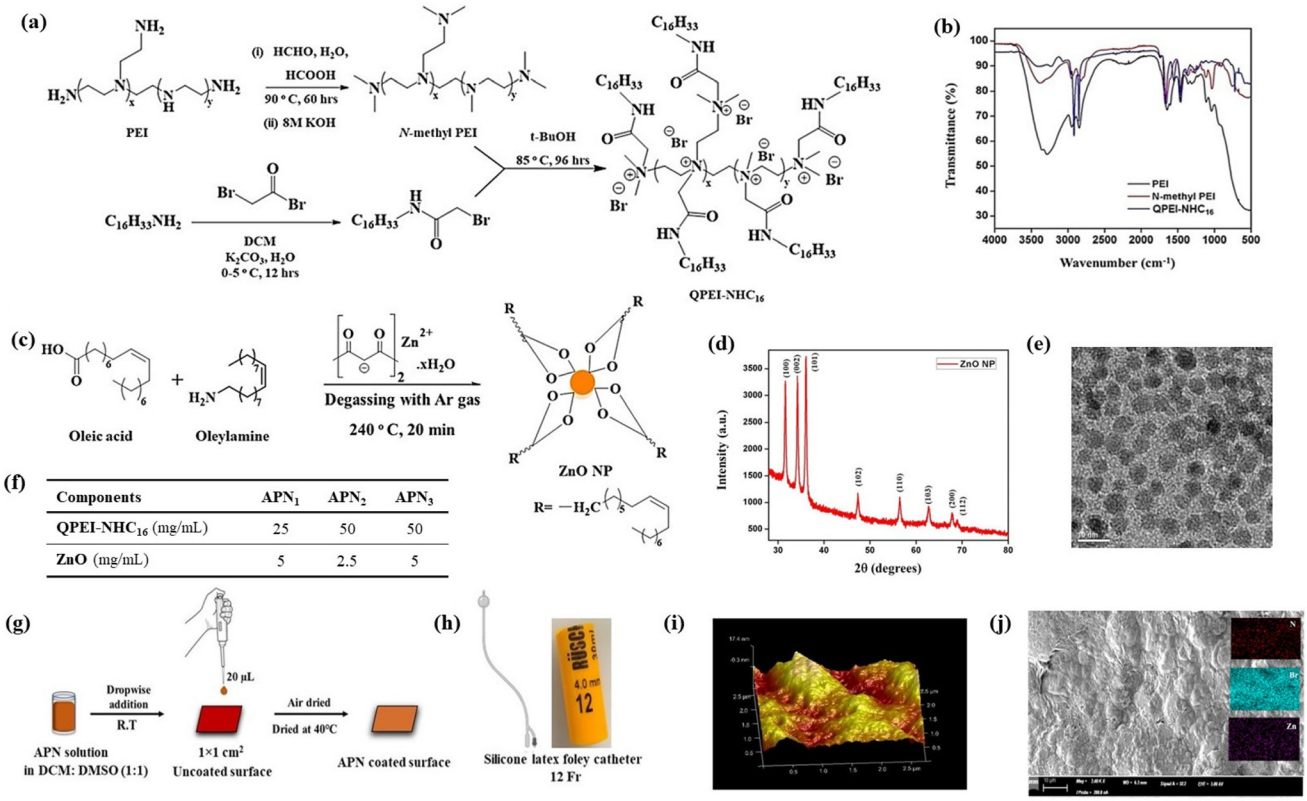

Fig. 1 (a) Synthesis of *N*-hexadecyl *N*-methyl PEI by *Eschweiler–Clarke* methylation of PEI, following quaternization with hexadecyl bromoethanamide; (b) Fourier transform IR spectra of PEI, *N*-methyl PEI and QPEI-NHC_{16}; (c) synthesis of zinc oxide nanoparticles; (d) X-ray diffraction pattern of ZnO nanoparticles; (e) transmission electron microscopy imaging of ZnO nanoparticles; scale bar = 10 nm; (f) concentrations of the two components in the antimicrobial nanocomposite formulations (APNs); (g) schematic representation of coating of antimicrobial polymer nanocomposite (APN) solution onto silicone surfaces by the drop-casting method; (h) representative image of a Foley catheter (Rusch catheter of thickness = 12 Fr) used for experiments; (i) atomic force microscopy image of silicone surfaces coated with APN_3 in height phase; (j) energy dispersive X-ray analysis of APN_3 coated silicone surface. Inset images represent colour mapping of nitrogen (red), bromine (blue) and zinc (purple). Scale bar = 250 µm.

mixing equivolume ratios of polymer solution in DCM and ZnO solution in DMSO, to yield three different formulations with varying concentrations of the components (Fig. 1f), namely, APN_1 (25 mg mL^{-1} of QPEI-NHC_{16} and 5 mg mL^{-1} of ZnO), APN_2 (50 mg mL^{-1} of QPEI-NHC_{16} and 2.5 mg mL^{-1} ZnO) and APN_3 (50 mg mL^{-1} of QPEI-NHC_{16} and 5 mg mL^{-1} ZnO). 20 µL of the different APN solutions were then uniformly dropcast onto the 1 × 1 cm^2 silicone surfaces (Fig. 1g). Uncoated surfaces were used as a control for comparison. Scanning electron microscopy was used to check the uniformity and presence of coating on silicone surfaces revealing the rough morphology of the coated surface. Furthermore, energy-dispersive X-ray analysis of the APN coated surface showed the presence of nitrogen, bromine, and zinc (Fig. 1j) Nitrogen and bromine corresponded to the presence of QPEI-NHC_{16}, while zinc was representative of the ZnO nanoparticles. Uncoated silicone surfaces showed the presence of only Si with a smooth morphology (Fig. S1e‡). For 12 Fr silicone catheters, cut into 3 cm lengths, dip-coating with APN_3 solution was executed (Fig. 1h), and the coated segments were characterized by FESEM (Fig. S1c and d‡). Atomic force microscopy confirmed a uniform coating and showed a root-mean-square (RMS) roughness of 1.94 nm for the coated surface (Fig. 1i).

Antibacterial activity for APN coated surfaces. The APN_1, APN_2, and APN_3 coated silicone surfaces were screened for antibacterial activity against representative Gram-positive (MRSA ATCC 33591) and Gram-negative (*E. coli* R3336) bacteria, by incubating 20 mL of ~5 × 10^6 CFU per mL bacterial suspension on the coated surfaces for 30 min. Then the surfaces were dragged on nutrient agar plates and the plates were incubated overnight to check the viability of pathogens. A similar experiment performed on the uncoated surface demonstrated thick bacterial lawns. APN_1 and APN_2 coated surfaces also displayed similar bacterial lawn growth, indicating their poor antibacterial property. However, the APN_3 coated surfaces showed effective killing, with no bacterial growth of MRSA and *E. coli* (Fig. 2a). The bacterial load on the surfaces contaminated with *E. coli* was also quantitatively assessed. While uncoated silicone surfaces had a burden of 5.47 log CFU per cm^2, the APN coated surfaces displayed a reduced bacterial burden, indicating their antibacterial potential. Out of the three formulations, APN_1 and APN_2 displayed a modest

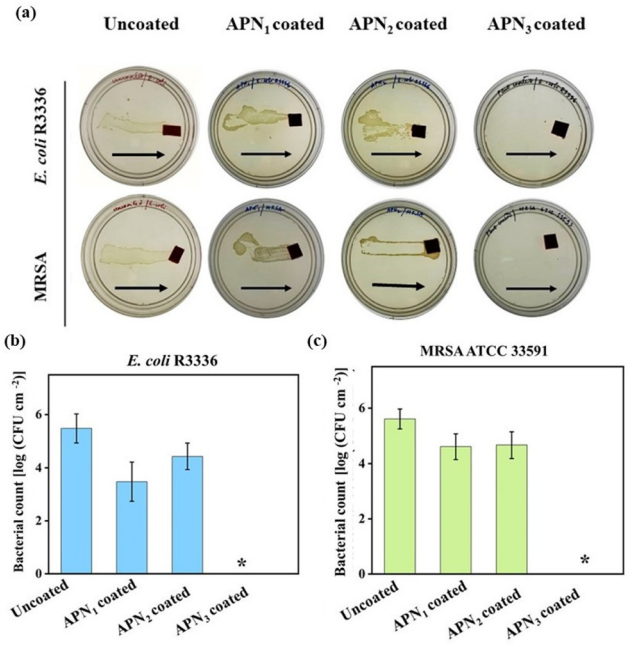

Fig. 2 Antibacterial activity of APN coated silicone surfaces; (a) antibacterial activity of APN coated silicone surface against *E. coli* R3336 and methicillin-resistant *S. aureus* (MRSA ATCC 33591). Arrows indicate the direction of dragging of surfaces on agar plates. Bacterial burden on APN coated surfaces against (b) *E. coli* R3336 and (c) MRSA ATCC 33591. An asterisk (*) indicates a bacterial count of <50 CFU per cm^2.

reduction of ~1 log CFU per cm^2 (bacterial burden for APN_1 = 3.47 log CFU per cm^2, for APN_2 = 4.42 log CFU per cm^2). The APN_3 coated surfaces, however, were highly bactericidal, and displayed complete killing (reduction of 5.47 log) (Fig. 2b). In the case of Gram-positive MRSA, APN_1 and APN_2 demonstrated a moderate antibacterial effect (bacterial burden for APN_1 = 4.6 log CFU per cm^2, for APN_2 = 4.7 log CFU per cm^2), with a similar ~1 log reduction as compared to uncoated surfaces (bacterial burden = 5.6 log CFU per cm^2). Here too, APN_3 coated surfaces displayed 100% killing of MRSA, with a reduction of 5.6 log bacteria (Fig. 2c). Based on these results, APN_3, exhibiting potent antibacterial properties, was chosen for subsequent experiments. While APN_1 and APN_2, with lower concentrations of the polymer and ZnO did not show complete bacterial killing, APN_3, with the highest concentration of both polymer and ZnO, was identified as the optimum formulation.

We further investigated the antibacterial activity of surfaces coated with APN_3 against different clinical isolates of Gram-positive bacteria *E. faecium* (VRE 903), *S. epidermidis* MTCC 3615 and MRSA ATCC 33591, along with Gram-negative bacteria *K. pneumoniae* R3934 and *K. pneumoniae* ATCC 700603 and compared the activity with surfaces coated with either the polymer (QPEI-NHC_{16}) or ZnO. It was observed that, the APN_3 coated surface effectively killed all tested bacteria whereas the uncoated surface, as well as surfaces coated with QPEI-NHC_{16} and ZnO, showed thick growth of a bacterial lawn (Fig. S2a‡). Quantitatively, the bacterial load on surfaces incubated with MRSA was also evaluated. Uncoated silicone surfaces exhibited a load of 3.9 log CFU per cm^2, QPEI-NHC_{16} and ZnO coated surfaces had a similar bacterial burden, showing their moderate antibacterial properties (bacterial burden for QPEI-NHC_{16} coated surface = 3.2 log CFU per cm^2 and ZnO coated surface = 4.01 log CFU per cm^2). However, APN_3 coated surfaces exhibited 100% killing of MRSA effectively (Fig. S2b‡).

To ascertain the efficacy of APN_3 coated silicone surfaces, they were checked against various drug-resistant strains of *E. coli* and *P. aeruginosa* R590 using a similar protocol. The uncoated surface showed the growth of a thick lawn of bacterial colonies, whereas, APN_3 coated surfaces showed complete killing against all tested bacterial strains, than the polymer-coated silicone surfaces with complete killing within just 30 min (Fig. 3a and Fig. S2c‡).[32]

To provide a quantitative assessment of bacterial reduction achieved by APN_3 coated surfaces, titration of viable bacterial cells was performed for *E. coli* R3336 and *P. aeruginosa* R590. Uncoated surfaces showed thick growth of bacteria (bacterial load = 4.1 log CFU per cm^2), whereas APN_3-coated surfaces demonstrated complete killing of *E. coli* R3336 bacteria with a reduction of 4.1 log as compared to the QPEI-NHC_{16} polymer coated surface, which showed average antibacterial activity of less than 1 log reduction in bacterial colonies (bacterial burden = 3.2 log CFU per cm^2), and ZnO coated surface (3.4 log CFU per cm^2; Fig. 3b). Antibacterial activity assessment against *P. aeruginosa* R590 for APN_3 coated surfaces showed the killing of 100% of bacterial cells, with a reduction of 3.3 log. QPEI-NHC_{16} and ZnO coated surfaces showed mediocre activity against *P. aeruginosa* bacteria with a bacterial burden of 3.9 log CFU per cm^2 and 3.7 log CFU per cm^2, respectively (Fig. 3c). The marked decrease in bacterial counts highlights the robust antibacterial efficacy of surfaces coated with APN_3 compared to surfaces coated with QPEI-NHC_{16} or ZnO across a wide range of bacteria. This underscores the potential utility of APN_3-coated surfaces in the prevention of catheter-associated urinary tract infections (CAUTIs).

To visually validate the effectiveness of APN_3-coated surfaces in killing bacteria, the surfaces were exposed to 20 μL of ~5×10^6 CFU per mL *E. coli* R3336 and *P. aeruginosa* R590 bacteria for 30 min. It was observed that for the uncoated surfaces as well as QPEI-NHC_{16} or ZnO coated surfaces, the nutrient media became turbid indicating the growth of bacteria. On the other hand, for APN_3-coated surfaces, media remained clear, demonstrating the absence of bacterial growth, and establishing the efficacy of the coating, with a rapid bactericidal effect within 30 min (Fig. 3d and e).

Bactericidal kinetics. Bacterial colonization of invasive biomedical devices can cause major life-threatening infections. Infections through catheters can spread during the handing of the catheters so it is important for surfaces to rapidly kill bacterial cells before the infection prevails.[33] To evaluate how fast bacterial cells can be eradicated, bactericidal kinetics was performed for the silicone surfaces coated with APN_3. Upon incubation of these surfaces with *E. coli* R3336, *E. coli* MTCC 443, and *P. aeruginosa* R590 stationary cells, the surfaces showed

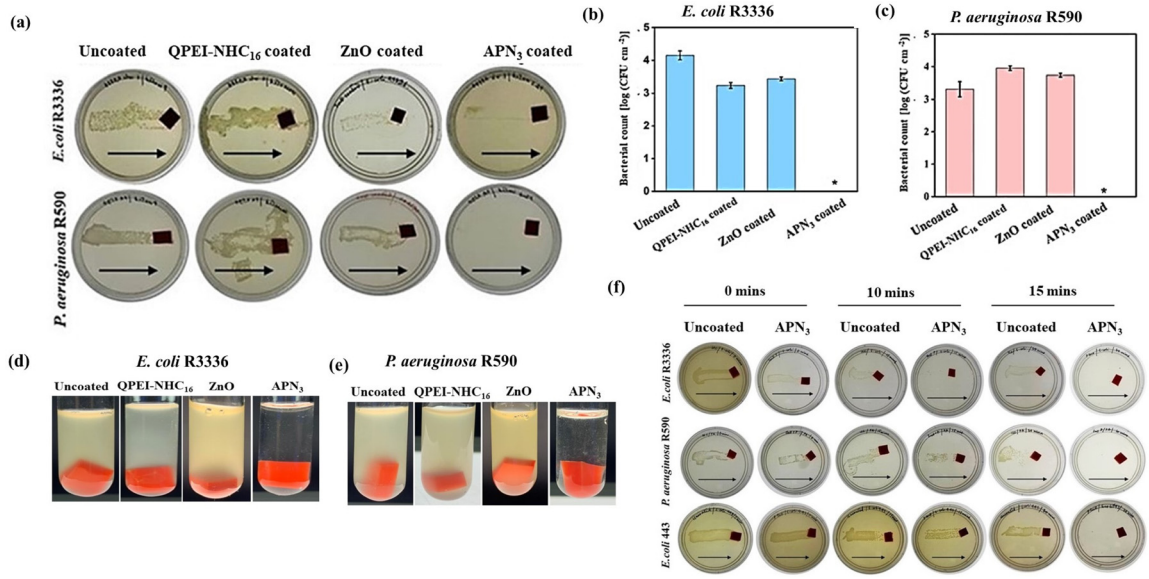

Fig. 3 (a) Potent killing of bacteria by the optimized coating APN_3 against key UTI-causing multi-drug resistant Gram-negative bacteria *E. coli* and *P. aeruginosa* through the dragging method. Arrows indicate the direction of dragging of surfaces on agar plates. Reduction in bacterial count for (b) *E. coli* R3336 and (c) *P. aeruginosa* R590. An asterisk (*) indicates a bacterial count of <50 CFU per cm^2 plates. Visualization of antibacterial activity through turbidity tests against (d) *E. coli* R3336 and (e) *P. aeruginosa* R590; (f) bactericidal kinetics of uncoated and APN_3 coated surfaces against *E. coli* R3336, *P. aeruginosa* R590 and *E. coli* MTCC 443. Arrows indicate the direction of dragging of surfaces on agar plates.

effective killing within 10–15 min (Fig. 3f). Such rapid bactericidal activity observed within much smaller time frames as compared to just the polymer indicates the synergistic efficacy of the nanocomposite. While the polymer coated glass surface itself is bactericidal, it requires higher concentrations and much longer time frames (24 h) to display complete killing.

Antibacterial activity of APN_3-coated urinary catheters. After affirming the ability of the APN_3 coated silicone surfaces to rapidly inactivate a wide range of bacteria upon exposure, the APN_3 coating was further validated on real catheters by dip-coating the 12 Fr urinary catheters, as described earlier. The catheter pieces were incubated with Gram-negative *E. coli* R3336; when incubated and dragged across the agar plate, a thick lawn of bacteria grew for the uncoated catheters (Fig. 4a). When quantitative assessment was done, uncoated catheters showed a high bacterial load (bacterial burden of 4.8 log CFU per cm^2) and QPEI-NHC_{16} coated surfaces showed a slight reduction (bacterial burden = 3.7 log CFU per cm^2). No bacterial colonies were observed in the case of APN_3 coated catheters. Counting of the bacterial load also validated the efficacy of APN_3 as ~4.8 log reduction in *E. coli* R3336 bacterial cells was observed (Fig. 4b).

Wash stability and retention of antibacterial activity of APN_3 coatings. Coatings on catheters can wash off due to repeated urination. Determining the stability of these coatings after washing is mandatory. The silicone surfaces coated with APN_3 were washed with saline repeatedly in 5 cycles by vortexing them for 1 min (Fig. S3a‡). SEM images and elemental mapping showing the presence of the elements of the coating confirmed that the coating was still present on the surfaces (Fig. S3b and c‡).

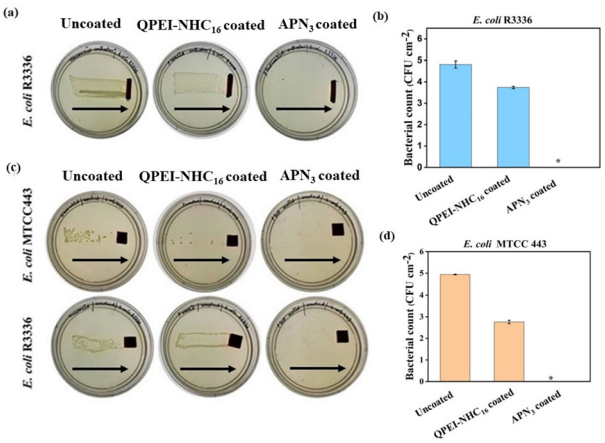

Fig. 4 (a) Antibacterial activity of uncoated silicone catheter and silicone catheters coated with QPEI-NHC_{16} and APN_3 against *E. coli* R3336 by the dragging method. Arrows indicate the direction of dragging of surfaces on agar plates; (b) reduction in bacterial load for uncoated, QPEI-NHC_{16} and APN_3 coated catheters; retention of antibacterial activity of APN_3 coated surfaces after multiple washes with saline (5 times) (c) through the dragging method and (d) through the determination of bacterial count. Asterisk (*) indicates a bacterial count of <50 CFU per cm^2.

The washed surfaces were checked for their antibacterial activity against *E. coli* R3336 and *E. coli* MTCC 443. It was observed that the uncoated control surfaces showed thick bacterial colonies whereas the APN_3 coated surfaces showed no growth of bacteria when dragged across agar plates (Fig. 4c). There was 100% killing of bacterial colonies of *E. coli* MTCC

443 by APN_3 coated surfaces, with a 4.9 log reduction. Even after multiple washing steps, the APN_3 coated surface retained its antimicrobial property and was capable of complete killing of the challenging bacterial load (Fig. 4d). The potent bactericidal property proves that washing does not strip the surfaces completely of their antibacterial property. The highly hydrophobic hexadecyl chain-bearing polymer is not soluble in water. This hydrophobicity may have a potential role in adhering the nanocomposite to the silicone surface, in addition to other non-covalent van der Waal type interactions such as hydrogen bonding within the film as well as with the surface. This in turn validates the stability of the APN_3 coating during multiple cycles of washing with saline.

Inhibition of biofilm formation on coated surfaces. The urinary tract, when equipped with a catheter, creates optimal circumstances for the substantial growth of biofilm communities. Various bacterial species form biofilms on indwelling catheters, leading to complications in patient care. Among these issues, crystalline biofilms pose a significant challenge by obstructing the catheter passage and causing episodes of pyelonephritis and septicemia.[34] A biofilm is a multi-cellular microbial structure made up of several metabolically inactive or dormant bacterial cells, an extracellular matrix that is self-produced, and antimicrobial diffusion barriers.[35–38] Furthermore, it was shown that dispersed cells originating from mature biofilm dispersion were distinct from planktonic and biofilm embedded bacterial cells.[11] Therefore, the ability of APN_3 to prevent bacterial biofilm growth against *E. coli* R3336, *E. coli* MTCC 443 and MRSA ATCC 33591 was next tested. Biofilm inhibition was studied for APN_3 coated surfaces, which were incubated with bacteria in biofilm inducing medium. Upon quantification of the biofilm embedded burden, the APN_3 coated surfaces showed a ~4 log reduction in cell viability in the case of *E. coli* MTCC 443 (bacterial burden 4.4 log CFU per mL), a ~3 log reduction for *E. coli* R3336 (bacterial burden 5.3 log CFU per mL) and a ~3 log reduction for MRSA biofilm (bacterial burden 5.8 log CFU per mL) indicating the potential of the APN_3 coating (Fig. 5a–c). QPEI-NHC_{16} coated surfaces showed a moderate reduction in biofilm bacterial burden for *E. coli* as well as MRSA biofilms with a bacterial burden of 7.3 log CFU per mL, 7.6 log CFU per mL and 7.7 log CFU per mL for *E. coli* MTCC 443, *E. coli* R3336 and MRSA biofilms, respectively.

On APN_3 coated surfaces, the extent of biofilm formation was visualized using CLSM imaging, after being stained with SYTO 9 and PI (Fig. 5d–f). Uncoated surfaces showed colossal

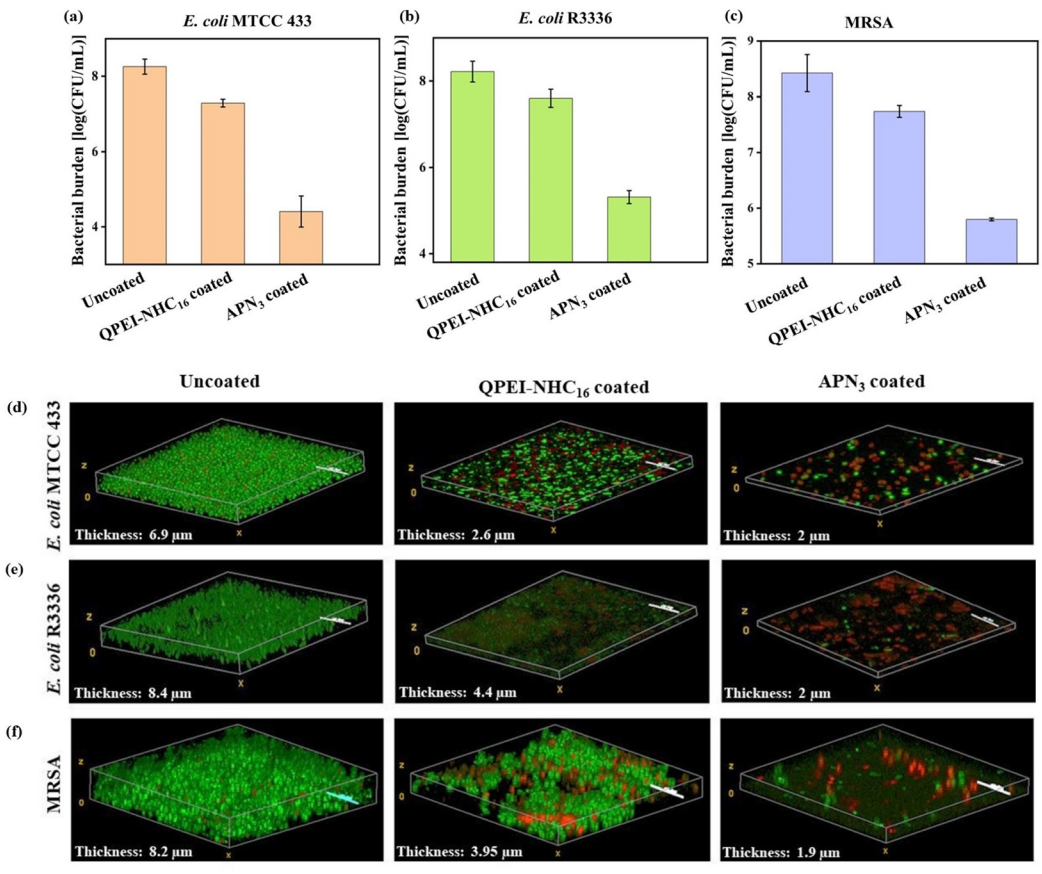

Fig. 5 Biofilm inhibition study for drug-resistant Gram-negative and Gram-positive bacteria; reduction in bacterial burden in (a) *E. coli* MTCC 443, (b) *E. coli* R3336 and (c) MRSA ATCC 33591 biofilm; CLSM images of PI-SYTO9 stained biofilms in uncoated, QPEI-NHC_{16} and APN_3 coated surfaces against (d) *E. coli* MTCC 443, (e) *E. coli* R3336 and (f) MRSA ATCC 33591 biofilm. Scale bar = 10 µm.

growth of bacterial biofilms with thicknesses of 8.4 μm, 6.9 μm and 8.2 μm for *E. coli* R3336, *E. coli* MTCC 443 and MRSA ATCC 33591, respectively. On the other hand, APN_3 coated surfaces showed a thickness of 2 μm in *E. coli* biofilms and 1.9 mm in the MRSA biofilm proving the efficacy of inhibiting the growth of biofilms on the surfaces. More importantly, as SYTO9-PI staining revealed, the APN_3 coated surfaces revealed a smattering of both SYTO9-PI-stained cells indicating a membrane compromised state. On the other hand, the uncoated surfaces had a thick lawn of SYTO9-only cells, indicating multiple layers of viable cells. These results were consistent across the three bacterial strains tested. The incorporation of ZnO nanoparticles significantly enhanced the biofilm inhibition properties of the coating, as coating with only the polymer did not reduce the biofilm thickness and cell burden as much as with the APN_3 coating.

Antifungal activity of coated surfaces. *Candida* species are commonly found in the human gastrointestinal system, vaginal tract, and skin.[39] During hospital stays, especially in the ICU, patients often develop risk factors, with candiduria being a common cause of fungal UTIs. *Candida*-related urinary tract infections are on the rise in hospitals, particularly in individuals with prolonged urinary catheterization. The significance of indwelling devices in hospitalized patients lies in the formation of complex biofilms on mucosal and plastic surfaces, comprising yeast, hyphae, and pseudo hyphae microcolonies. *Candida* species contribute to 78.3% of nosocomial fungal infections.[40]

The efficacy of the coating was checked against fluconazole-resistant *C. albicans* AB226 and *C. albicans* AB399. When contaminated with fungal suspension and incubated for 2 h, the APN_3 coated showed no fungal growth upon dragging on a YPD plate. On the other hand, uncoated surfaces showed thick lawns of fungi on the plate (Fig. 6a).

To quantify the antifungal activity, the coated and uncoated surfaces were incubated with a million viable fungal cells of both strains. The surfaces were washed with saline, and the solution was titered and plated for counting of the fungal colonies. After an incubation period of 2 h, APN_3 coated surfaces showed 100% killing of fungal cells with a 4.1 log reduction for *C. albicans* AB399 and a 4.3 log in the case of *C. albicans* AB226. The uncoated surfaces showed a burden of 4.1 log CFU per cm^2 and 4.3 log CFU per cm^2 (Fig. 6b). The nanocomposite was significantly superior to the individual components where QPEI-NHC_{16} coated (fungal load = 3.3 log CFU per cm^2) and ZnO coated (fungal load = 3.3 log CFU per cm^2) surfaces showed a ~1 log reduction in fungal colonies of *C. albicans* AB399. Similarly, for *C. albicans* AB226, QPEI-NHC_{16} coated (fungal load = 3.6 log CFU per cm^2) and ZnO coated (fungal load = 4.2 log CFU per cm^2) surfaces did not show much antifungal activity in 2 h.

Fungicidal kinetics. To avoid fungal colonization and eventual biofilm formation, it is mandatory to rapidly eradicate fungi from catheter surfaces. It is important to measure how fast the APN_3 coating can eradicate fungal strains. The surfaces were incubated with *C. albicans* AB226 and *C. albicans* AB399

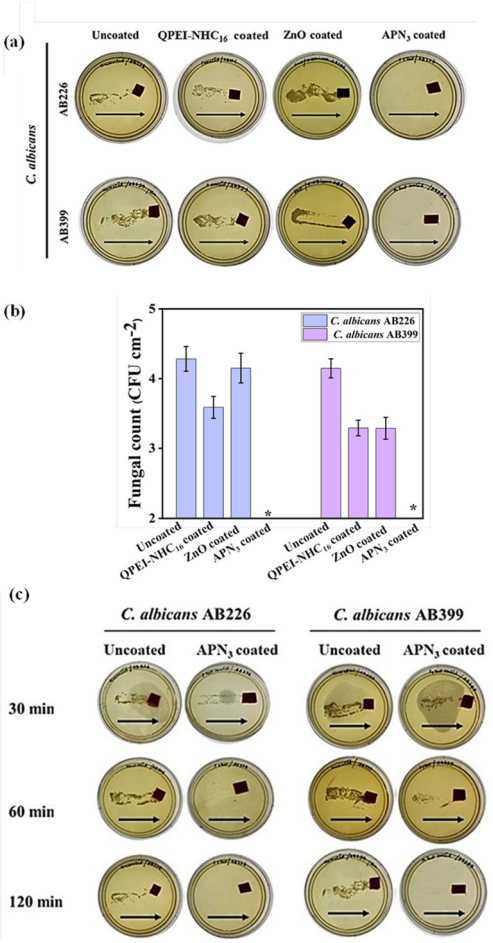

Fig. 6 Antifungal activity of coated surfaces against the drug-resistant fungi *C. albicans* AB226 and *C. albicans* AB399 determined (a) through the dragging method, (b) reduction in fungal count and (c) fungicidal kinetics of uncoated and APN_3 coated surfaces; arrows indicate the direction of dragging of surfaces on YPD agar plates. An asterisk (*) indicates a fungal count of <50 CFU per cm^2.

at different time points of 30 min, 1 h, and 2 h. The coating effectively killed *C. albicans* AB226 within 1 h whereas *C. albicans* AB399 took 2 h to be killed. Within 1–2 h, the coating killed 100% of the fungal strains, demonstrating its higher effectiveness against fungal strains (Fig. 6c).

Assessment of APN_3 antibacterial effectiveness against UTI causing pathogens. Human urine is contaminated with various pathogens during UTIs, mostly uropathogenic *E. coli* (UPEC). When UPEC enters the bladder, it meets uroepithelial cells and triggers a powerful innate immune response by activating many signalling pathways and these bacteria are usually resistant to common antibiotics.[4,41] Antibacterial activity against hospital acquired UPEC CFT073 was checked, and it showed 100% killing with a 4.8 log reduction in bacterial burden in saline in the case of APN_3. The surfaces coated with either QPEI-NHC_{16} polymer or ZnO displayed little or no activity against *E. coli* CFT073 in saline, with bacterial burdens of 3.6 log CFU per cm^2 and 4.4 log CFU per cm^2, respectively,

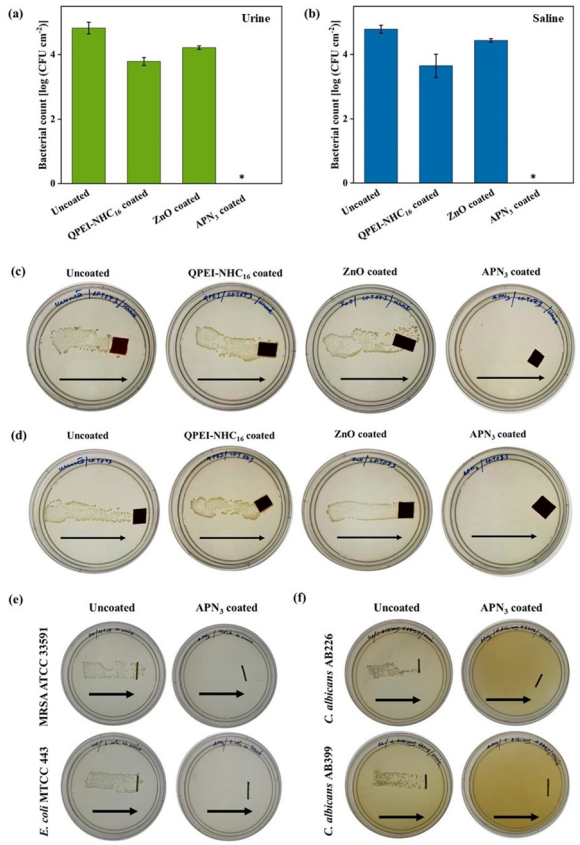

Fig. 7 Antimicrobial activity of APN_3 coated surfaces and catheters against uropathogenic bacteria and fungi in urine. Reduction in the bacterial count of *E. coli* CFT073 on coated surfaces when inoculated in (a) urine and (b) saline; antibacterial activity determined through the dragging method of surfaces incubated with bacterial suspensions prepared in (c) urine and (d) in saline; (e) antibacterial activity of uncoated and APN_3 coated catheters against MRSA and *E. coli* inoculated in human urine; (f) antifungal activity of uncoated and APN_3 coated catheters incubated with fungal suspension prepared in urine. An asterisk (*) indicates a fungal count of <50 CFU per cm^2. Arrows indicate the direction of dragging of surfaces on agar plates.

as compared to the uncoated surface (bacterial burden of 4.8 log CFU per cm^2; Fig. 7b). To further mimic the real UTI situation, urine from a healthy donor was collected and contaminated with UPEC CFT073. The antibacterial efficacy of the surfaces was checked when *E. coli* CFT073 was inoculated in urine and saline by dragging surfaces across the agar plate. Uncoated surfaces, as well as QPEI-NHC_{16} and ZnO coated surfaces, showed thick bacterial lawn growth whereas APN_3 coated surfaces showed no bacterial colonies on the agar plate (Fig. 7c and d). Furthermore, upon quantitative assessment it was observed that APN_3 coated surfaces showed 100% killing of bacterial cells in 30 min with a ~4.8 log reduction compared to QPEI-NHC_{16} (bacterial burden = 3.8 log CFU per cm^2) and ZnO coated surfaces (4.2 log CFU per cm^2), which showed mediocre antibacterial activity against UPEC CFT073 when inoculated in urine (Fig. 7a).

During implantation, catheters can get contaminated due to poor procedural practices. During a UTI, human urine contains a huge fungal and bacterial load that can attach to the catheter and form impenetrable biofilms.[8] It is important to prevent any possible pathogen in the urine from adhering to the surface. To assess that, urinary catheters were inoculated with both Gram-positive MRSA and Gram-negative *E. coli* bacteria (Fig. 7e) and two strains of *Candida albicans* (Fig. 7f) in urine. For the surfaces, when dragged across respective nutrient and YPD agar plates, it was observed that there were thick colony growths in the case of uncoated surfaces, whereas no colonies were observed for APN_3 coated surfaces showing effective killing of pathogens.

Mechanism of action. Membrane active nature of coated surface was determined through different methods.[36] To have a better understanding of the mechanism of killing of bacteria by APN_3, the bacterial morphology of *E. coli* MTCC 443 was visualized by scanning electron microscopy after incubation with APN_3 coated polystyrene surfaces. Images of the cells incubated with the uncoated surfaces demonstrated the presence of a well-defined morphology and *E. coli* bacteria with a rod-like morphology (Fig. 8a). On the other hand, coated surfaces showed the disruption of the bacterial cells, indicating loss of structural integrity of the bacterial cells, and debris was observed, affirming membrane disruption. To further visualize the membrane disruption of bacteria, a live–dead assay was done. Dual-staining microscopic imaging with SYTO-9 and PI dyes was adopted to assess membrane perturbation by coated surfaces (Fig. 8b). The appearance of green fluorescence validated that practically all bacteria were alive in the case of uncoated surfaces. However, upon exposure to the coating, merged green and red fluorescence from SYTO-9 and PI staining was observed. The permeabilization of PI into these cells indicated their membrane compromised nature.

Cytoplasmic membrane depolarization. ZnO has been reported to decrease cytoplasmic bacterial cell potential under certain conditions. While ZnO can induce depolarization of the bacterial cytoplasmic membrane, it is also possible for it to mitigate or counteract depolarization in some scenarios.[42,43] In certain cases, higher concentrations of ZnO might not induce depolarization, but instead exhibit protective effects on the membrane potential.[44] $DiSC_3(5)$ accumulates on hyperpolarized membranes, and due to self-quenching, does not show significant fluorescence. If the membrane potential is lost, and the membrane gets depolarized, the dye moves out from the membrane into the solution, where we see a strong increment in fluorescence. For QPEI-NHC_{16} coated wells, the fluorescence intensity increased over time. Due to the decrease in depolarization effects of ZnO, the APN_3 coating showed an average value increment in depolarization of ZnO and QPEI-NHC_{16}. As a result, this discovery plainly demonstrated that APN_3 had disrupted the normal membrane potential (Fig. 8c).

Cytoplasmic inner membrane permeability. ZnO and a highly positively charged polymer like QPEI-NHC_{16} can cause physical damage to the cytoplasmic inner membrane, leading to increased membrane permeability. This increased permeability can result in the leakage of ions, small molecules,

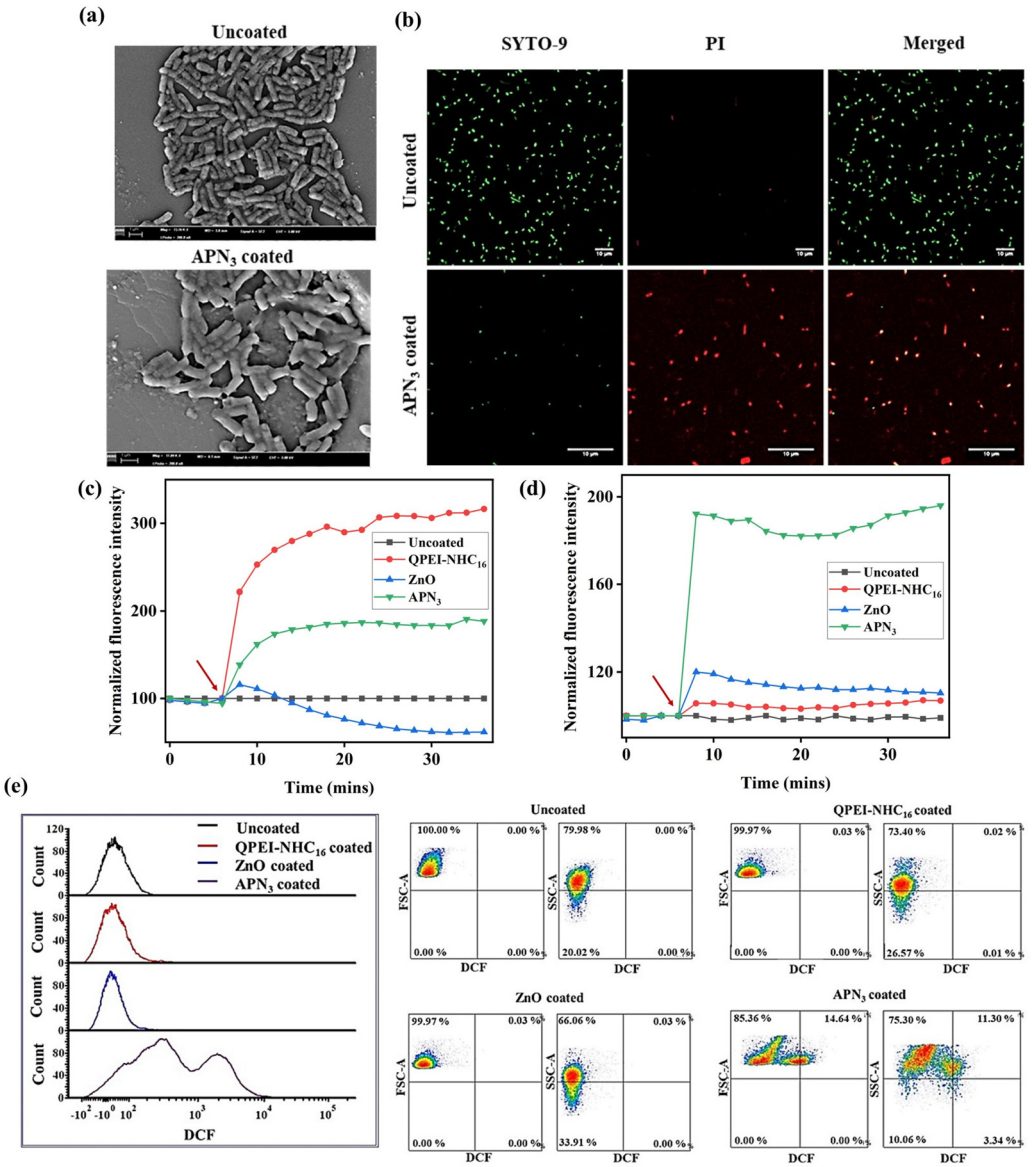

Fig. 8 Mechanistic investigations into the bactericidal action of APN_3 coating; (a) scanning electron images of *E. coli* MTCC 443 were used to track the death of bacteria. Scale bar = 10 μm. (b) Live–dead assay images of bacterial killing. Scale bar = 10 μm. (c) Cytoplasmic inner membrane permeability of planktonic *E. coli* MTCC 443 bacteria; (d) cytoplasmic membrane depolarization of *E. coli* MTCC 443; red arrow indicates the transfer of bacterial suspension with dye from control wells to coated wells. (e) Flow cytometric analysis of intracellular ROS in *E. coli* MTCC 443, generated upon incubation onto uncoated silicone surface, and QPEI-NHC_{16}, ZnO and APN_3 coated silicone surfaces.

and cellular components, disrupting the normal functioning of the bacterial cell.[45,46] The membrane permeabilizing capacity of APN_3 coated surfaces was assessed by employing PI dye, which exhibited increased fluorescence when it penetrated compromised bacterial cells and bound tightly to bacterial DNA. Compared to QPEI-NHC_{16} and ZnO coated surfaces, the APN_3 coated surface showed an enhanced effect on inner membrane permeability through the enhanced fluorescence observed, indicating disruption of the inner membrane of the bacteria (Fig. 8d).

Intracellular ROS generation in bacteria. Reactive oxygen species are deadly weapons to that can kill pathogens directly by causing oxidative stress or through various non-oxidative mechanisms.[47,48] We have observed that nanocomposite coatings are much superior in their bactericidal effect as compared to only polymer coatings. This indicates that the presence of ZnO is crucial for potent and rapid antibacterial activity. Referring to earlier reports on metal oxide nanoparticles, we anticipated a role for reactive oxygen species (ROS) in the bactericidal activity of the nanocomposite coating. $DCFH_2$ upon oxidation due to ROS generation turns into membrane permeable DCF (2′,7′-dichlorodihydrofluorescein), which is detected by flow cytometry.[49] The uncoated surface showed no ROS generation, whereas the QPEI-NHC_{16} coated surface

showed a very low percentage of ROS generation. ZnO, with inherent ROS generating properties, showed 2.1% intracellular ROS generation in 10 min. However, the polymer–nanocomposite system, APN_3, due to the synergistic effect of the polymer and metal oxide nanoparticle showed a high amount of ROS generation with a bimodal population distribution amounting to 50.3% to kill the bacterial cells in 10 minutes.[50] This asserts that a plausible reason for the rapid antimicrobial activity showed by the APN_3 coating is fast ROS generation, which can inactivate bacterial cells rapidly with along with the membrane disrupting activity of the polymer (Fig. 8e). Overall, a mechanistic investigation indicates the superior activity of the dual-component formulation for the inactivation of microbial cells. These preliminary investigations into the mechanism of action conclusively indicate the strong synergy between the quaternary hydrophobic polymer, which interacts with and perturbs the microbial envelope, and the inorganic zinc oxide nanoparticles, validating the superiority of the nanoformulation.

Antibacterial activity against metabolically suppressed bacterial cells

The prevalence of metabolically repressed stationary phase and persister cells, which are inert to typical antibiotic therapies, is one of the alarming challenges in healthcare settings. Therefore, as a result, if antibiotic treatment is discontinued, these cells may cause infections to return. Along with activity against planktonic bacteria, APN_3 coated surfaces also demonstrated potent activity against stationary phase *E. coli* cells. While uncoated surfaces showed the presence of a huge number of bacterial cells on the agar plates, APN_3 displayed complete killing of the dormant stationary phase bacterial cells, with no growth of any bacterial colonies on the plate (Fig. 9b).

Along with stationary phase cells, pathogenic bacteria also display persistent phenotypes, which are a small subpopulation of bacteria that can outlast antibiotic treatment by entering a dormant state. This subpopulation, known as persister cells, while not being conventionally resistant to antibiotics, can evade antibiotic action, and be rejuvenated when antibiotic therapy is discontinued, leading to recalcitrance of infection.[24,51,52] We assessed the bactericidal potential of our coated surfaces against *E. coli* persister cells generated by high dose ampicillin therapy.[53] APN_3-coated surfaces effectively killed these notorious antibiotic-persister *E. coli* cells within 30 min while uncoated and polymer-coated surfaces displayed substantial bacterial growth. This result underscored the efficacy of the APN_3 coating at eliminating difficult-to-eradicate subpopulations of bacteria (Fig. 9b).

Antimicrobial action against polymicrobial biofilms. The dearth of market-available antimicrobials, such as antibiotics and antifungals, against polymicrobial biofilms, which cause a slew of deadly illnesses such as CAUTIs, diabetic foot ulcers, lung infections, pulmonary disorders, and soft tissue infections, is a big challenge. The coexistence of *E. coli* and *Candida albicans* results in the development of polymicrobial biofilms, which are not completely curable even after several antibiotic treatments.[39] As a result, antimicrobial agents that are effective against such multispecies infections are in great demand. The dual efficacy of the APN_3 coating against both fungi and bacteria motivated us to check the efficacy of the coating against polymicrobial biofilms. The ability of APN_3 to inhibit the formation of polymicrobial biofilms of *E. coli* MTCC 443 and *Candida albicans* AB226 was tested (Fig. 9a). APN_3 reduced the fungal load by ~1.8 log with a fungal count of 5.4 log CFU per mL as compared to uncoated surfaces (fungal burden of 7.7 log CFU per mL) and the bacterial count by ~1.5 log with a bacterial burden of 7.1 log CFU per mL as compared to an uncoated surface (bacterial load of 8.9 log CFU per mL). This demonstrates the relevance of the polymer–nanocomposites' combined effectiveness of the cationic polymer and ZnO nanoparticles.

In vivo biocompatibility

To determine the biocompatibility of the polymer nanocomposite APN_3, it was coated onto medical grade silicone catheters and subsequently implanted into the subcutaneous pocket of mice (Fig. 10a). After periods of 3 days and 7 days, the mice were sacrificed and the tissue surrounding the implant was collected and examined for inflammatory responses, if any, through histological analysis using haematoxylin and eosin staining. Hematoxylin stains cell nuclei a purplish blue, and eosin stains the extracellular matrix and cytoplasm pink, with other components taking on various tints, hues, and colour combinations. The uncoated catheter showed moderate infiltration of inflammatory cells, mainly neutrophils and mononuclear cells, after 3 days (Fig. 10b). However, the tissues surrounding the implanted APN_3 coated catheter showed mild infiltration of inflammatory cells mainly neutrophils and mononuclear cells and a healthy keratin layer as indicated (Fig. 10b). After 7 days, the tissues showed no inflammatory response to the coated implant compared to the tissues surrounding the uncoated catheter, proving the coated one to be more biocompatible. This moderate improvement in the inflammatory response towards the implant compared to

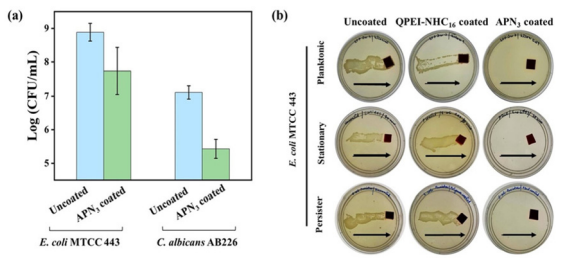

Fig. 9 Inhibition of polymicrobial biofilms on APN_3 coated surfaces. (a) Reduction in count of biofilm-embedded *C. albicans* AB226 and *E. coli* MTCC443 by APN_3; (b) antibacterial activity of uncoated surface and QPEI-NHC_{16} and APN_3 coated surfaces against planktonic, stationary and persister cells of *E. coli* MTCC 443 by dragging across the agar plate. Arrows indicate the direction of dragging of surfaces on agar plates.

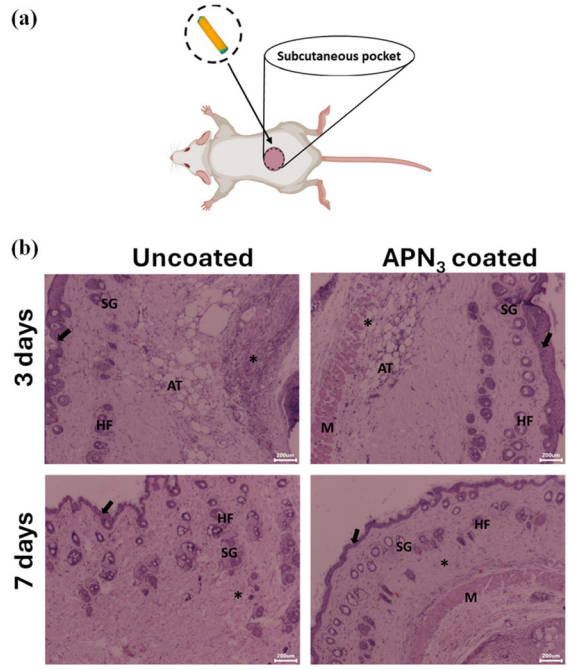

Fig. 10 *In vivo* biocompatibility of APN_3 coated catheters. (a) Representative image of catheter implantation in the subcutaneous pocket of the mouse. (b) *In vivo* biocompatibility of the coating. Histopathology analysis of tissues harvested from mice with an uncoated catheter implant and an APN_3 coated catheter implant upon haematoxylin and eosin staining shows sweat and sebaceous glands (SG), hair follicles (HF), adipose tissue (AT), muscle layer (M), keratin layer formation (arrow) and inflammatory response (asterisk). Scale bar = 200 μm.

the pristine catheter can be ascribed to the presence of zinc oxide, as evidenced in recent reports, which have proved that ZnO has anti-inflammatory properties.[54–57]

Conclusions

Prolonged catheterization fosters biofilm formation on the catheter surface, complicating treatment due to the growing prevalence of multidrug-resistant bacteria with the ability to create biofilms on catheters. Through this study, we developed a non-covalent paint-like coating based on the polymer nanocomposite APN_3. The coating was fabricated from organo-solutions of an antimicrobial polymer, QPEI-NHC_{16}, and ZnO nanoparticles. The dual active nanocomposite coating exhibited rapid bactericidal action against uropathogenic *E. coli* within 10 minutes, along with broad spectrum antimicrobial efficacy against drug-resistant Gram-positive, Gram-negative bacteria as well as pathogenic fungi, which are responsible for CAUTIs. Additionally, this coating demonstrates stability against multiple washes and inhibits the formation of single species and polymicrobial biofilms on catheter surfaces. Mechanistic investigations were carried out to validate the membrane disruption exhibited by the coatings and the generation of reactive oxygen species in a rapid manner through synergistic effects. Notably, it swiftly eradicates metabolically repressed stationary phase and persister cells of *E. coli*; this highlights its superior antibacterial properties. These attributes highlight the unique multifunctionality and novelty of this nanocomposite coating on urinary catheters. Taken together, the rapid bactericidal property of the coating, and biofilm inhibition, make the coating highly suitable as a preventive and therapeutic intervention for urinary catheters and mitigation of CAUTIs. Our validation of the coatings' stability and retention of activity on washing, and effective antimicrobial properties when coated onto urinary catheters, further buttresses the significance of this report. The coating also proved to have no inflammatory response with excellent biocompatibility *in vivo*. Altogether, the overall results suggest that the antimicrobial polymer nanocomposite coating has immense potential for further development as a multipronged strategy for reducing and tackling CAUTIs.

Methods

Synthesis

***N*-Hexadecyl-2-bromoethanamide.** 1-Aminohexadecane (64 mmol) and an aqueous solution of K_2CO_3 (95 mmol) were added to DCM (55 mL). The mixture was then cooled to 5 °C followed by dropwise addition of bromoacetyl bromide (95 mmol) solution in anhydrous DCM (55 mL). The mixture was stirred for 30 min. The mixture was then allowed to stir at room temperature for 18 h. The DCM layer was collected. The aqueous layer was washed using DCM (250 mL) twice. After that, the DCM solutions were mixed, and rinsed with water three times (100 mL each time). The DCM solution was then passed over anhydrous sodium sulphate (Na_2SO_4) and reduced in volume using a rotary evaporator to obtain a colourless solid product. The product was characterized through ^{1}H-NMR and FT-IR.

***N*-Methyl branched PEIs.** Polyethyleneimine (PEI) (750 kDa; 5.6 g) was taken in a round-bottom flask and formic acid (3.4 mL) was added followed by the addition of formaldehyde (5.45 mL) and 20 mL of water. The reaction mixture was refluxed at 90 °C for 60 h. The mixture was then cooled to room temperature followed by the addition of KOH (8 M) solution until the pH was ~11. The product was extracted by washing the mixture with chloroform. The product was characterized through ^{1}H-NMR and IR.

***N*-Hexadecyl, *N*-methyl PEIs.** *N*-Methyl PEI (17.5 mmol per repeating unit) was reacted with *N*-hexadecyl-2-bromoethanamide (26.3 mmol) in *tert*-butanol (50 mL) in a screw-top tube for 96 h at 75 °C. The resulting reaction mixture was reduced in volume using a rotary evaporator. Then, an excess of diethyl ether was added to obtain a pale-brown product. After settling of the precipitate, excess diethyl ether was decanted. The product was redissolved in chloroform and reprecipitated using diethyl ether thrice to remove any impurities. Finally, the precipitate was dried under vacuum to obtain the quater-

nized PEI (QPEI-NHC_{16}). The product was characterized through ^{1}H-NMR and FT-IR.

ZnO nanoparticles. Using zinc acetylacetonate monohydrate (6 mmol) as a metal precursor, zinc oxide nanoparticles (ZnO NP) were synthesized in the presence of oleyl amine (18 mmol) and oleic acid (3.6 mmol). The degassed mixture was heated under argon flux at 240 °C for 20 min.[31] After cooling, ethanol was used to precipitate the nanocrystalline product. The product was centrifuged. The product was purified using re-dispersion in chloroform and reprecipitation with ethanol. The nanoparticles showed high dispersibility in chloroform. A white powder was obtained after drying under vacuum.

Characterization of ZnO nanoparticles

X-ray diffraction (XRD). Zinc oxide nanoparticles (ZnO NP) were dispersed in chloroform (10 mg mL^{-1}) and dropcast on a 2 × 2 cm^2 glass slide, dried and studied by XRD spectroscopy using a Rigaku powder XRD instrument. Transmission electron microscopy (TEM). Zinc oxide nanoparticles were dispersed in chloroform (0.2 mg mL^{-1}) and dropcast on a TEM grid and the images were captured on a JEOL JEM 2100 Plus instrument operating at an acceleration of 200 kV. Fourier transform infrared spectroscopy (FT-IR) was done to characterize the ZnO NPs. To determine the size of the ZnO NPs, 20 particles were taken into consideration randomly from the TEM image, and using ImageJ analysis the average size of the particles was calculated. ZnO NPs were directly used for FT-IR measurements.

Coating of surfaces and characterization. An organic solution of QPEI-NHC_{16} was prepared in DCM at concentrations 100 mg mL^{-1} (91 wt%) and 10 mg mL^{-1}. ZnO NPs (9 wt%) were dispersed in DMSO and called APN_3. Employing these previously mentioned solutions, antimicrobial polymer nanocomposites (APN) of varying composition were prepared (Fig. 2a). APN_1 was synthesized by mixing equi-volumes of 50 mg mL^{-1} QPEI-NHC_{16} (83 wt%) and 10 mg mL^{-1} ZnO NP (17 wt%) whereas APN_2 was obtained through an equi-volume mixture of 100 mg mL^{-1} QPEI-NHC_{16} (95 wt%) and 5 mg mL^{-1} ZnO NP (5 wt%). Silicone surfaces (thickness ~0.3 mm) were cut into 1 × 1 cm^2 pieces and washed with isopropanol and water followed by rinsing with acetone to remove impurities. After the surfaces were dried, 20 μL of the previously prepared APN solution was dropcast on the surfaces and dried at room temperature and then at 40 °C. The APN coated surfaces were characterized through field emission scanning electron microscopy (FESEM), energy dispersion X-ray (EDX), and atomic force microscopy (AFM) as follows. 12 Fr silicone catheters were cut into small pieces of 3 cm in length, and dip coated with APN_3 (equivolume solutions of 100 mg mL^{-1} QPEI-NHC_{16} and 10 mg mL^{-1} ZnO) and characterized by FESEM.

Characterization of coated surfaces

Field emission scanning electron microscopy (FESEM). Uncoated and APN coated surfaces were characterized by FESEM studies with gold-sputtering before imaging.

Energy dispersive X-ray (EDX). The Zeiss Gemini 500 FESEM apparatus, which was carrying the EDX unit, was used to conduct an EDX analysis of the silicone samples. The samples were subjected to gold sputtering before imaging.

Atomic force microscopy (AFM). Si wafers were coated with APN_3 at a concentration of 20 μg mm^{-2} for QPEI-NHC_{16} and 0.4 μg mm^{-2} for ZnO NPs. Measurements were done using a Bruker Innova instrument with a silicon cantilever in tapping mode with frequencies between 300 and 400 kHz and spring constant values between 40 and 80 Nm^{-1}. Uncoated surfaces were used as a control.

Thermal stability of coatings. QPEI-NHC_{16} and ZnO NPs were examined for thermal stability under an N_2 gas flow at a rate of 40 mL min^{-1} with a temperature interval of 5 °C through thermogravimetric analysis (TGA) using a PerkinElmer STA 6000 instrument.

Antibacterial activity determined by the dragging method. APN_1, APN_2 and APN_3 coated silicone surfaces were checked for their antibacterial activity against Gram-positive MRSA ATCC 33591 and Gram-negative *E. coli* R3336.[58] Briefly mid-log phase bacteria were harvested after culturing at 37 °C for 6 h in nutrient media under constant shaking conditions. The bacteria were diluted in saline to obtain a concentration of ~5 × 10^6 CFU per mL, which was further used for experimentation. Onto the coated and uncoated surfaces, a 20 μL drop of the previously prepared bacterial suspension was placed and incubated for 30–45 min at 37 °C. The surfaces were then dragged across the nutrient agar plate along its diameter and incubated for 18 h. The agar plates were subjected to photographic imaging. Furthermore, to quantify viable bacterial cells on the surfaces, the surfaces were washed rigorously with 990 μL of saline. The wash solutions were then diluted serially 10-fold followed by dropping 20 μL of the dilutions onto nutrient agar plates. The agar plates were incubated for 18 h at 37 °C and colonies were counted. The experiment was done in triplicate.

Stability of APN_3 coating towards washing. 1 × 1 cm^2 silicone surfaces and 3 cm long catheter surfaces were coated through the drop-casting and dipping-methods, respectively, with the APN_3 solution. The surfaces were washed in 5 cycles with saline through vortexing for 2 min for every wash. The washed surfaces were then characterized by scanning electron microscopy and energy-dispersive X-ray spectroscopy. Gold sputtering was done before imaging.

Activity against multidrug-resistant (MDR) bacteria. Different clinical isolates of Gram-positive bacteria *E. faecium* ATCC 19634, vancomycin-resistant *E. faecium* 903 (VRE 903) and MRSA ATCC 33591, along with Gram-negative bacteria *K. pneumoniae* R3934 and *E. coli* R3336 were checked for antibacterial activity. The bacteria were cultured at 37 °C for 6 h in nutrient media under constant shaking conditions. *E. faecium* was cultured in brain heart infusion (BHI) medium under the same conditions. The bacterial suspension was diluted to ~5 × 10^6 CFU per mL suspension in saline. 20 μL of this bacterial suspension was dropped on the 1 × 1 cm^2 surfaces of silicone coated with QPEI-NHC_{16}, ZnO and APN_3. In the experiment, uncoated silicone surfaces were used as the control. The silicone surfaces were dragged across the nutrient agar plate's diameter following a 30 min incubation period at 37 °C. The

plates were then imaged after incubation for 18 h at 37 °C. The viable bacterial colonies were also counted on the surfaces following the previously mentioned protocol.[21,23] The experiment was done in triplicate.

Antibacterial activity through visual turbidity tests. *E. coli* R3336 and *P. aeruginosa* R590 were grown in nutrient media for 6 h under continuous shaking conditions. The bacterial suspensions were diluted to ~5×10^6 CFU per mL in saline. QPEI-NHC_{16} and APN_3 coated surfaces were incubated by placing a 20 μL drop of bacterial suspension on top. After incubation for 30 min, these surfaces were transferred to freshly prepared growth media and incubated at 37 °C for 18 h. The uncoated surfaces were treated as the control for the experiment. After incubation, the turbidity of the media was investigated visually, if any, and photographs were captured. The experiment was done in duplicate.

Activity against various *E. coli* cells

Activity against planktonic cells. *E. coli* R3336, *E. coli* MTCC 443, *E. coli* ATCC 25922, *E. coli* MTCC 448, *E. coli* R250, and *E. coli* 4806 cells were cultured at 37 °C for 6 h in nutritional media under continual shaking conditions. The bacterial suspension was diluted in saline to obtain ~5×10^6 CFU per mL suspensions. 20 μL of these bacterial suspensions were put onto the coated and uncoated surfaces. The remainder of the experiment was as mentioned previously. The experiment was done in triplicate.

Activity against stationary cells. *E. coli* MTCC 443 cells were grown to the stationary phase by diluting a mid-log phase bacterial culture ~1000-fold in nutrient broth and incubating it at 37 °C for 16 h under shaking conditions. The stationary cells were centrifuged for 3 min at 9000 rpm and resuspended in saline. The suspension was further diluted in saline to obtain ~5×10^5 CFU per mL suspensions of stationary cells. This suspension was used to investigate the antibacterial activity. The procedure employed was like that of the antibacterial assay of coated surfaces as mentioned previously. The experiment was done in triplicate.

Activity against persister cells. *E. coli* MTCC443 cells were grown into persisters following a previously reported protocol.[35] Briefly, the stationary cells were centrifuged and treated with 300 μg mL^{-1} ampicillin solution and incubated at 37 °C for 4 h under shaking conditions. The bacterial suspension was then centrifuged at 9000 rpm for 3 min and resuspended in saline. The final resuspension was done to obtain a concentration of around 5×10^5 CFU per mL. The procedure that followed was similar to the antibacterial assay of coated surfaces against planktonic cells. The experiment was done in triplicate.

Bactericidal kinetics. Mid-log phase *E. coli* R3336 (~5×10^6 CFU per mL) cells were diluted with saline (~10^5 CFU per mL). A 20 μL aliquot of this bacterial suspension was dropped onto 1 × 1 cm^2 silicone coated with QPEI-NHC_{16} and APN_3. Uncoated silicone surfaces were employed as a control. The samples were incubated at 37 °C for varying time intervals of 0, 5, 10, 15, 30, and 45 min. Following an incubation period of 18 h at 37 °C, these surfaces were dragged over the nutrient agar plates along their diameter, incubated and photographed. The experiment was done in triplicate.

Antibacterial activity of APN_3 coated urinary catheters. A 12 Fr silicone catheter was cut into small pieces (25–30 mg) of 3 cm in length. Both ends of the catheters were blocked by heat-sealing them. The catheter surfaces were dip-coated with APN_3 and after air-drying, they were further dried at 45 °C. A droplet of 20 μL of ~10^6 CFU per mL *E. coli* R3336 bacterial suspension in saline was placed on a Petri dish. The surfaces were rubbed on the bacteria to smear the entire surface of the catheter. Uncoated catheters were used as controls. The catheter surfaces were incubated at 37 °C for 45 min. Following incubation, the catheter surfaces were dragged on agar plates and incubated at 37 °C for 18 h. The plates were then photographed and the viable bacterial colonies were also counted as mentioned previously. The experiment was done in triplicate.

Retention of antibacterial activity after multiple washes. The uncoated and coated catheters and silicone surfaces were washed with saline in 5 cycles for 1 min each. After washing the surfaces, they were incubated with 20 μL ~5×10^6 CFU per mL *E. coli* R3336 and *E. coli* MTCC 443 bacteria at 37 °C for 30 min. The procedure followed thereafter was similar to that mentioned previously. The experiment was done in triplicate.

Biofilm inhibition study

Confocal laser scanning microscopy. Glass coverslips of 18 mm in diameter were coated with QPEI-NHC_{16} and APN_3. The coated coverslips were transferred to the wells of a 6-well plate. Uncoated cover slips were used as controls. MRSA ATCC 33591, *E. coli* MTCC 443, and *E. coli* R3336 cells were suspended in the appropriate medium (M9 medium with 0.02% casamino acid and 0.5% glycerol was used for *E. coli* biofilms and nutrient broth supplemented with 1% NaCl and 1% glucose was used for the MRSA biofilm). 2 mL of bacterial suspension was then added to the wells containing the coverslips. The 6-well plates were incubated at 37 °C for 72 h under stationary conditions for *E. coli* R3336 and *E. coli* MTCC 443 biofilms and 24 h for the MRSA biofilm. Consequently, the coverslips were removed and washed with saline. The coverslips were then placed on glass slides, followed by the addition of a solution of SYTO 9 green dye (60 μM) and PI red dye (15 μM) and covered with another coverslip and incubated for 15 min. The biofilms grown, if any, were then photographed using a confocal laser scanning microscope (Zeiss LSM 800). The experiment was done in triplicate.

Bacterial colony counting. QPEI-NHC_{16} and APN_3 coated surfaces were used in the experiment. The experiment employed uncoated glass slips as the control. Biofilms were allowed grow on the coated or uncoated coverslip surfaces following the previously mentioned method. The coverslips were then washed with saline to remove unadhered cells and placed in a new 6-well plate. The biofilms were then digested using trypsin EDTA (1 : 4 for MRSA and 1 : 10 for *E. coli*). This digestion solution was then further diluted 10-fold using saline and 20 μL of the resulting dilutions were drop-plated on nutrient

agar plates. The agar plates were incubated for 18 h at 37 °C, consequently the bacterial colonies were counted. The experiment was done in triplicate.

Anti-fungal activity of coated surfaces. On 1 × 1 cm^2 coated and uncoated surfaces, 20 μL of a 10^6 CFU per mL fungal suspension of *C. albicans* AB226 and AB399 was dropped and incubated at 37 °C for 2 h. YPD (yeast peptone dextrose) agar plates were used in the subsequent procedure, which was identical to the previously mentioned protocol for examining the antibacterial activity. Viable fungal colonies upon exposure to coated and uncoated surfaces were also counted following the previously mentioned protocol. The experiment was done in triplicate.

Fungicidal kinetics. The fungicidal kinetics of the coated and uncoated surfaces were investigated against *C. albicans* AB226 and *C. albicans* AB399. The procedure followed was similar to that of bactericidal kinetics mentioned earlier. The time points studied in the experiment were 0 min, 30 min, 1 h and 2 h. The experiment was done in triplicate.

Antibacterial activity of surfaces against *E. coli* CFT073. To check the efficacy of the coated and uncoated surfaces against UPEC *E. coli* CFT073, the bacteria were cultured in nutrient broth for 6 h. A bacterial suspension of ~5 × 10^6 CFU per mL was taken in saline and urine separately. The surfaces were incubated with 20 μL of the bacterial suspension at 37 °C for 30 min. The surfaces were dragged across the agar plates and incubated for 18 h at 37 °C. The plates were photographed, and the viable colonies were counted as in the above-mentioned procedure.

Antimicrobial activity of urinary catheters in urine. The efficacy of the coated and uncoated catheters against Gram-positive MRSA and Gram-negative *E. coli* MTCC 443 bacteria as well as *C. albicans* AB226 and AB399 fungal strains were checked in urine. The uncoated and APN_3 coated polyurethane catheters were incubated with bacterial and fungal suspension of 20 μL of ~5 × 10^6 CFU per mL for 30 min, at 37 °C. The catheters were then dragged across nutrient agar and YPD agar plates for bacterial colony and fungal colony growth and incubated at 37 °C for 18 h. The plates were then photographed. Urine was collected with informed consent from a healthy donor, following the protocols permitted by the Institutional Ethics Committee (IEC) of the Jawaharlal Nehru Centre for Advanced Scientific Research (JNCASR) (JNC/IEC/M3-2022/JH-001) under the guidelines of the Indian Council of Medical Research (ICMR), by the Government of India (GoI).

Mechanism of action

Membrane disruption through scanning electron microscopy. Polystyrene well-plates were coated with APN_3. Uncoated wells were considered as controls. The wells were then filled with 400 μL aliquots of a bacterial suspension of *E. coli* R3336 at ~10^7 CFU per mL in saline and incubated at 37 °C for 2 h. The bacteria were then harvested in a centrifuge tube and centrifugation was carried out at 3000 rpm for 5 min. The resulting bacterial pellet was resuspended in 30%, 50%, 70%, and 90% ethanol : water solutions. Final resuspension was in 90% ethanol and 5 μL of the suspension was dropcast onto a silicon wafer and air-dried. The samples were gold-sputtered before imaging with a Zeiss Gemini 500 FESEM instrument.

Membrane disruption through fluorescence microscopy (live–dead assay). Wells of a 96-well plate were coated with APN_3. Uncoated wells were treated as controls. 100 μL of ~10^7 CFU per mL bacterial suspension of *E. coli* MTCC 443 was dropped into 10 wells and incubated at 37 °C for 60 min. The bacterial suspensions were then collected in a centrifuge tube and centrifuged at 5000 rpm for 5 min. The supernatant was discarded and resuspended in 1 mL of saline. SYTO-9 (3 μM) and PI (15 μM) were added and left for 15 min in the dark. The dye-supplemented bacterial suspension was centrifuged again at 5000 rpm for 5 min. The supernatant was discarded and redissolved in 100 μL saline. 5 μL was dropcast on a glass slide for imaging and covered with a coverslip. The experiment was done in triplicate.

Intracellular ROS generation through flow cytometry. Surfaces coated with QPEI-NHC_{16}, ZnO and APN_3 solutions were incubated with 20 μL of ~10^7 CFU per mL bacterial suspension of *E. coli* MTCC 443 at 37 °C for 10 min. Right after incubation, the surfaces were washed with 1 mL saline. Pristine surfaces were treated as controls in the experiment. The washed solutions were treated with 10 μL of 10 μM 2′,7′-dichlorodihydrofluorescein diacetate (DCFDA) dye for staining. The samples were analysed for intracellular ROS (reactive oxygen species) generation with proper excitation and emission of DCFDA dye through flow cytometry in the FACS Aria II device. Gating and analysis were done using FCS Express 6 software.

Membrane depolarization assay. Polystyrene 96-well plates were coated with APN_3, QPEI-NHC_{16} and ZnO. Uncoated wells were considered as the control for the experiment. *E. coli* MTCC 443 cells in the mid-log phase were collected, centrifuged at 3500 rpm for 5 min and washed with a 1 : 1 ratio of 100 mM KCl and HEPES buffer (pH 7.4) followed by a 1 : 1 ratio of 5 mM glucose and HEPES buffer. The cells were then resuspended in a solution containing 5 mM HEPES buffer, 100 mM KCl with 0.2 mM EDTA, and 5 mM glucose. EDTA was added to enable dye take up by permeabilizing the outer membrane of *E. coli*. EDTA is a chelating agent that can disrupt the integrity of the outer membrane, making it more permeable. The presence of EDTA in the resuspension buffer helps to facilitate this permeabilization process. In the experiment, the *E. coli* cells were treated with the fascinating dye 3,3′-dipropylthiadicarbocyanine iodide, also known as DiSC3(5), at a concentration of 2 μM. The cells were incubated with this dye along with 190 μL of bacterial suspension on a plate and incubated for 45 min. Fluorescence was measured at intervals of 2 min over a period of 30 min in the Tecan Spark plate reader. After the first 4 min the bacterial suspensions were transferred from the uncoated wells to the respective coated wells for fluorescence intensity measurements.

Inner membrane permeabilization assay. Similar to the membrane depolarization assay, the coated 96-well plate was

used. *E. coli* MTCC 443 cells in the mid-log phase were separately subjected to centrifugation (3500 rpm, 5 min), followed by washing with a 1 : 1 ratio of 100 mM KCl and HEPES buffer solution and finally resuspended in a 1 : 1 ratio of 5 mM glucose and HEPES buffer (pH 7.4). The working concentrations of the bacteria were approximately 10^8 CFU per mL. Next, 190 μL portions of bacterial suspension containing 10 μM propidium iodide (PI) were added to the wells of a Corning 96-well black plate with a clear bottom. The fluorescence of PI was monitored for 4 min using an excitation wavelength of 535 nm and an emission wavelength of 617 nm after which the bacterial suspensions treated with dye were transferred from the uncoated well to the respective coated wells for a period of 30 min for fluorescence measurement in the Tecan Spark microplate reader.

Polymicrobial inhibition activity. Glass coverslips of 18 mm in diameter were coated with APN_3, and pristine surfaces were used as the control for the experiment. The coating's activity against polymicrobial biofilms was tested using interkingdom mixed biofilms of *Candida albicans* and *E. coli*. Individual cultures of *C. albicans* AB226 and *E. coli* MTCC 443 were diluted in an equi-volume combination of potato dextrose broth (PDB) and tryptic soy broth (TSB) to reach bacterial and fungal concentrations of 10^5 and 10^6 CFU per mL, respectively.[11] Then, 2 mL of this mixed mixture was transferred to the wells of a fresh 6-well plate, where the coated and uncoated coverslips were placed. Plates were incubated for 24 hours at 37 °C. After that, the coverslips were washed with saline. Following dilution, 20 L of each diluted solution was dropped on nutritional agar plates containing amphotericin B (100 g mL^{-1}) in the case of *E. coli*. *C. albicans* was grown on YPD agar plates with vancomycin (150 g mL^{-1}). The bacterial plates were then incubated for 24 hours at 37 °C and the fungal plates for 48 hours at 30 °C to count the number of live colonies. The experiment was done in triplicate.

Determination of *in vivo* biocompatibility of coated catheters. The *in vivo* animal experiments were done by following the appropriate protocols, which were approved and permitted by the Institutional Animal Ethics Committee (IAEC) of the Jawaharlal Nehru Centre for Advanced Scientific Research (JNCASR) (201/Go/ReBi/S/2000/CPCSEA) under the national laws of the Committee for the Purpose of Control and Supervision of Experiments on Animals (CPCSEA) by the Government of India (GoI). One group of mice was implanted with uncoated catheters and the other group was implanted with APN_3-coated catheters. Four mice were used in each group. The animals were sedated with a combination of ketamine (40 mg kg^{-1}) and xylazine (2 mg kg^{-1} xylazine). All the mice were bred in the institute's animal facility. Before, the experiment was conducted, the fur in the dorsal line was removed and a small incision was made into the subcutaneous pocket of the mice. Medical grade silicone catheters were cut into small pieces of 0.5 cm in length and the ends were heat sealed. The catheter pieces were inserted into the subcutaneous pocket. The incisions were then sutured up with vicryl sutures. After 3 days, the mice were sacrificed, and the adjacent tissues were collected and placed in a formalin solution. The tissues were washed and subsequently dehydrated using 70, 90 and 100% ethanol solution for 1 h. The tissues were then checked for inflammatory response through haematoxylin and eosin staining method.

Author contributions

The work and the experiments were designed by D. P. and J. H. Biofilm inhibition and microscopy studies were done by S. M. Flow cytometry studies for ROS determination were performed by R. M. All other studies were conducted by D. P., S. G., Y. A. and J. H. All the data were analyzed by D. P., S. G., S. M., Y. A., R. M., and J. H. The manuscript was written by D. P., S. G., S. M., Y. A., R. M., and J. H. All the authors approved the final version of the manuscript.

Conflicts of interest

There are no conflicts to declare.

Acknowledgements

J. H. acknowledges JNCASR, the Sheikh Saqr Laboratory, the Ras Al Khaimah Centre for Advanced Materials and Raknor LLC for financial support. Y. A. acknowledges CSIR for a research fellowship.

References

1 M. Medina and E. Castillo-Pino, An introduction to the epidemiology and burden of urinary tract infections, *Ther. Adv. Urol.*, 2019, **11**, 1756287219832172.
2 W. E. Stamm and S. R. Norrby, Urinary tract infections: disease panorama and challenges, *J. Infect. Dis.*, 2001, **183**, S1–S4.
3 B. Bhattacharjee, S. Ghosh, D. Patra and J. Haldar, Advancements in release-active antimicrobial biomaterials: A journey from release to relief, *Wiley Interdiscip. Rev.: Nanomed. Nanobiotechnol.*, 2022, **14**, e1745.
4 A. L. Flores-Mireles, J. N. Walker, M. Caparon and S. J. Hultgren, Urinary tract infections: epidemiology, mechanisms of infection and treatment options, *Nat. Rev. Microbiol.*, 2015, **13**, 269–284.
5 D. M. Siddiq and R. O. Darouiche, New strategies to prevent catheter-associated urinary tract infections, *Nat. Rev. Urol.*, 2012, **9**, 305–314.
6 S. L. Percival, L. Suleman, C. Vuotto and G. Donelli, Healthcare-associated infectionsmedical devices and biofilms: risk, tolerance and control, *J. Med. Microbiol.*, 2015, **64**, 323–334.
7 L. E. Nicolle, Catheter associated urinary tract infections, *Antimicrob. Resist. Infect. Control*, 2014, **3**, 23.

8 M. Kostakioti, M. Hadjifrangiskou and S. J. Hultgren, Bacterial biofilms: development, dispersal, and therapeutic strategies in the dawn of the post antibiotic era, *Cold Spring Harbor Perspect. Med.*, 2013, **3**, a010306.
9 A. L. Flores-Mireles, J. N. Walker, T. M. Bauman, A. M. Potretzke, H. L. Schreiber, A. M. Park, J. S. Pinkner, M. G. Caparon, S. J. Hultgren and A. Desai, Fibrinogen Release and Deposition on Urinary Catheters Placed during Urological Procedures, *J. Urol.*, 2016, **196**, 416–421.
10 M. M. Konai, B. Bhattacharjee, S. Ghosh, J. Haldar, M. M. Konai, B. Bhattacharjee, S. Ghosh and J. Haldar, Recent progress in polymer research to tackle infections and antimicrobial resistance, *Biomacromolecules*, 2018, **19**, 1888–1917.
11 S. Ghosh, R. Mukherjee, S. Mukherjee, S. Barman and J. Haldar, Engineering antimicrobial polymer nanocomposites: in situ synthesis, disruption of polymicrobial biofilms, and *in vivo* activity, *ACS Appl. Mater. Interfaces*, 2022, **14**, 34527–34537.
12 Y. Acharya, S. Bhattacharyya, G. Dhanda and J. Haldar, Emerging Roles of Glycopeptide Antibiotics: Moving beyond Gram-positive Bacteria, *ACS Infect. Dis.*, 2022, **8**, 1–28.
13 S. M. Jacobsen, D. J. Stickler, H. L. T. Mobley and M. E. Shirtliff, Complicated catheter-associated urinary tract infections due to *Escherichia coli* and *Proteus mirabilis*, *Clin. Microbiol. Rev.*, 2008, **21**, 26–59.
14 S. Ghosh, S. Mukherjee, D. Patra and J. Haldar, Polymeric biomaterials for prevention and therapeutic intervention of microbial infections, *Biomacromolecules*, 2022, **23**, 592–608.
15 S. Ghosh and J. Haldar, Cationic polymer–based antibacterial smart coatings, in *Advances in smart coatings and thin films for future industrial and biomedical engineering applications*, Elsevier, 2020, pp. 557–582.
16 G. Dhanda, R. Mukherjee, D. Basak and J. Haldar, Small-Molecular Adjuvants with Weak Membrane Perturbation Potentiate Antibiotics against Gram-negative Superbugs, *ACS Infect. Dis.*, 2022, **8**, 1086–1097.
17 C. Ghosh, V. Yadav, W. Younis, H. Mohammad, Y. A. Hegazy, M. N. Seleem, K. Sanyal and J. Haldar, Aryl-alkyl-lysines: Membrane-Active Fungicides That Act against Biofilms of *Candida albicans*, *ACS Infect. Dis.*, 2017, **3**, 293–301.
18 P. Singha, J. Locklin and H. Handa, A review of the recent advances in antimicrobial coatings for urinary catheters, *Acta Biomater.*, 2017, **50**, 20–40.
19 S. Ghosh, L. Jolly and J. Haldar, Polymeric paint coated common-touch surfaces that can kill bacteria, fungi and influenza virus, *MRS Commun.*, 2021, 1–9.
20 B. W. Trautner and R. O. Darouiche, Role of biofilm in catheter-associated urinary tract infection, *Am. J. Infect. Control*, 2004, **32**, 177–183.
21 Y. Acharya, K. K. Taneja and J. Haldar, Dual functional therapeutics: mitigating bacterial infection and associated inflammation, *RSC Med. Chem.*, 2023, **14**, 1410–1428.
22 J. Haldar, A. K. Weight and A. M. Klibanov, Preparation, application and testing of permanent antibacterial and antiviral coatings, *Nat. Protoc.*, 2007, **2**, 2412–2417.
23 J. Haldar, D. An, L. Alvarez de Cienfuegos, J. Chen and A. M. Klibanov, Polymeric coatings that inactivate both influenza virus and pathogenic bacteria, *Proc. Natl. Acad. Sci. U. S. A.*, 2006, **103**, 17667–17671.
24 J. Hoque, P. Akkapeddi, C. Ghosh, D. S. S. M. Uppu and J. Haldar, A Biodegradable Polycationic Paint that Kills Bacteria *in Vitro* and *in Vivo*, *ACS Appl. Mater. Interfaces*, 2016, **8**, 29298–29309.
25 A. Kumar, P. K. Vemula, P. M. Ajayan and G. John, Silver-nanoparticle-embedded antimicrobial paints based on vegetable oil, *Nat. Mater.*, 2008, **7**, 236–241.
26 G. T. Werneburg, A. Nguyen, N. S. Henderson, R. R. Rackley, D. A. Shoskes, A. L. Le Sueur, A. T. Corcoran, A. E. Katz, J. Kim, A. J. Rohan and D. G. Thanassi, The Natural History and Composition of Urinary Catheter Biofilms: Early Uropathogen Colonization with Intraluminal and Distal Predominance, *J. Urol.*, 2019, **203**, 357–364.
27 S. Saint, J. A. Meddings, D. Calfee, C. P. Kowalski and S. L. Krein, Catheter-associated urinary tract infection and the Medicare rule changes, *Ann. Intern. Med.*, 2009, **150**, 877–884.
28 J. C. Nickel, J. Downey and J. W. Costerton, Movement of pseudomonas aeruginosa along catheter surfaces. A mechanism in pathogenesis of catheter-associated infection, *Urology*, 1992, **39**, 93–98.
29 J. Hoque, S. Ghosh, K. Paramanandham and J. Haldar, Charge-Switchable Polymeric Coating Kills Bacteria and Prevents Biofilm Formation *in Vivo*, *ACS Appl. Mater. Interfaces*, 2019, **11**, 39150–39162.
30 V. B. Schwartz, F. Thétiot, S. Ritz, S. Pütz, L. Choritz, A. Lappas, R. Förch, K. Landfester and U. Jonas, Antibacterial Surface Coatings from Zinc Oxide Nanoparticles Embedded in Poly(N-isopropylacrylamide) Hydrogel Surface Layers, *Adv. Funct. Mater.*, 2012, **22**, 2376–2386.
31 A. Sirelkhatim, S. Mahmud, A. Seeni, N. H. M. Kaus, L. C. Ann, S. K. M. Bakhori, H. Hasan and D. Mohamad, Review on Zinc Oxide Nanoparticles: Antibacterial Activity and Toxicity Mechanism, *Nano-Micro Lett.*, 2015, **7**, 219–242.
32 C. Valotteau, N. Baccile, V. Humblot, S. Roelants, W. Soetaert, C. V. Stevens and Y. F. Dufrêne, Nanoscale antiadhesion properties of sophorolipid-coated surfaces against pathogenic bacteria, *Nanoscale Horiz.*, 2019, **4**, 975–982.
33 D. J. Stickler, Bacterial biofilms in patients with indwelling urinary catheters, *Nat. Clin. Pract. Urol.*, 2008, **5**, 598–608.
34 S. Mukherjee, S. Barman, R. Mukherjee and J. Haldar, Amphiphilic Cationic Macromolecules Highly Effective Against Multi-Drug Resistant Gram-positive Bacteria and Fungi with No Detectable Resistance, *Front. Bioeng. Biotechnol.*, 2020, **8**, 55.

35 R. Dey, K. De, R. Mukherjee, S. Ghosh and J. Haldar, Small antibacterial molecules highly active against drug-resistant *Staphylococcus aureus*, *MedChemComm*, 2019, **10**, 1907–1915.
36 R. Ron, D. Zbaida, I. Z. Kafka, R. Rosentsveig, I. Leibovitch and R. Tenne, Attenuation of encrustation by self-assembled inorganic fullerene-like nanoparticles, *Nanoscale*, 2014, **6**, 5251–5259.
37 M. M. Konai and J. Haldar, Lysine-Based Small Molecule Sensitizes Rifampicin and Tetracycline against Multidrug-Resistant *Acinetobacter baumannii* and *Pseudomonas aeruginosa*, *ACS Infect. Dis.*, 2020, **6**, 91–99.
38 J. R. Gaston, A. O. Johnson, K. L. Bair, A. N. White and C. E. Armbruster, Polymicrobial interactions in the urinary tract: is the enemy of my enemy my friend?, *Infect. Immun.*, 2021, **89**, IAI.00652-20.
39 C. A. Kauffman, Diagnosis, and management of fungal urinary tract infection, *Infect. Dis. Clin. North Am.*, 2014, **28**, 61–74.
40 V. C. Thompson, P. J. Adamson, J. Dilag, D. Bandara, K. Srikantharajah, A. Blok, A. V. Ellis, D. L. Gordon and I. Köper, Biocompatible anti-microbial coatings for urinary catheters, *RSC Adv.*, 2016, **6**, 53303–53309.
41 P. Surwade, T. Luxton, J. Clar, F. Xin and V. Shah, Impact of the changes in bacterial outer membrane structure on the anti-bacterial activity of zinc oxide nanoparticles, *J. Nanopart. Res.*, 2020, **22**, 1–8.
42 N. Babayevska, Ł. Przysiecka, I. Iatsunskyi, G. Nowaczyk, M. Jarek, E. Janiszewska and S. Jurga, ZnO size and shape effect on antibacterial activity and cytotoxicity profile, *Sci. Rep.*, 2022, **12**, 8148.
43 S. Gharpure, R. Yadwade and B. Ankamwar, Non-antimicrobial and Non-anticancer Properties of ZnO Nanoparticles Biosynthesized Using Different Plant Parts of Bixaorellana, *ACS Omega*, 2022, **7**, 1914–1933.
44 K. S. Siddiqi, A. Rahman, T. Tajuddin and A. Husen, Properties of zinc oxide nanoparticles and their activity against microbes, *Nanoscale Res. Lett.*, 2018, **13**, 141.
45 S. V. Gudkov, D. E. Burmistrov, D. A. Serov, M. B. Rebezov, A. A. Semenova and A. B. Lisitsyn, A mini review of antibacterial properties of ZnO nanoparticles, *Front. Phys.*, 2021, **9**, 884.
46 M. Levy, C. M. Courtney, P. P. Chowdhury, Y. Ding, E. L. Grey, S. M. Goodman, A. Chatterjee and P. Nagpal, Assessing different reactive oxygen species as potential antibiotics: selectivity of intracellular superoxide generation using quantum dots, *ACS Appl. Bio Mater.*, 2018, **1**, 529–537.
47 C. N. Paiva and M. T. Bozza, Are reactive oxygen species always detrimental to pathogens?, *Antioxid. Redox Signal.*, 2014, **20**, 1000–1037.
48 E. Eruslanov and S. Kusmartsev, Identification of ROS using oxidized DCFDA and flow-cytometry, *Methods Mol. Biol.*, 2010, **594**, 57–72.
49 A.-L. Heins, T. Johanson, S. Han, L. Lundin, M. Carlquist, K. V. Gernaey, S. J. Sørensen and A. E. Lantz, Quantitative Flow Cytometry to Understand Population Heterogeneity in Response to Changes in Substrate Availability in *Escherichia coli* and *Saccharomyces cerevisiae* Chemostats, *Front. Bioeng. Biotechnol.*, 2019, **7**, 187.
50 J. Hoque, P. Akkapeddi, V. Yadav, G. B. Manjunath, D. S. S. M. Uppu, M. M. Konai, V. Yarlagadda, K. Sanyal and J. Haldar, Broad spectrum antibacterial and antifungal polymeric paint materials: synthesis, structure-activity relationship, and membrane-active mode of action, *ACS Appl. Mater. Interfaces*, 2015, **7**, 1804–1815.
51 J. Hoque, U. Adhikary, V. Yadav, S. Samaddar, M. M. Konai, R. G. Prakash, K. Paramanandham, B. R. Shome, K. Sanyal and J. Haldar, Chitosan Derivatives Active against Multidrug-Resistant Bacteria and Pathogenic Fungi: *In Vivo* Evaluation as Topical Antimicrobials, *Mol. Pharm.*, 2016, **13**, 3578–3589.
52 M. M. Konai, U. Adhikary, S. Samaddar, C. Ghosh and J. Haldar, Structure-Activity Relationship of Amino Acid Tunable Lipidated Norspermidine Conjugates: Disrupting Biofilms with Potent Activity against Bacterial Persisters, *Bioconjugate Chem.*, 2015, **26**, 2442–2453.
53 H. Agarwal and V. Shanmugam, A review on anti-inflammatory activity of green synthesized zinc oxide nanoparticle: Mechanism-based approach, *Bioorg. Chem.*, 2020, **94**, 103423.
54 M. Nilavukkarasi, S. Vijayakumar and S. Prathipkumar, Capparis zeylanica mediated biosynthesized ZnO nanoparticles as antimicrobial, photocatalytic and anticancer applications, *Mater. Sci. Energy Technol.*, 2020, **3**, 335–343.
55 Z. M. Ramadhania, J. Nahar, J. C. Ahn, D. U. Yang, J. H. Kim, D. W. Lee, B. M. Kong, R. Mathiyalagan, E. J. Rupa, R. Akter, D. C. Yang, S. C. Kang and G.-Y. Kwak, *Terminalia ferdinandiana* (Kakadu Plum)-Mediated Bio-Synthesized ZnO Nanoparticles for Enhancement of Anti-Lung Cancer and Anti-Inflammatory Activities, *Appl. Sci.*, 2022, **12**, 3081.
56 S. Karakus, E. Tan, M. Ilgar, Y. M. Sahin, D. S. Mansuroglu, D. Ismik, R. A. Somroo and A. Kilislioglu, Swelling behaviour, rheological property and drug release profile of the anti-inflammatory drug metamizole sodium from xanthan gum–ZnO nanoparticles, *Polym. Bull.*, 2022, **79**, 357–380.
57 S. Ghosh, R. Mukherjee, D. Basak and J. Haldar, One-Step Curable, Covalently Immobilized Coating for Clinically Relevant Surfaces That Can Kill Bacteria, Fungi, and Influenza Virus, *ACS Appl. Mater. Interfaces*, 2020, **12**, 27853–27865.
58 S. Mukherjee, S. Ghosh and J. Haldar, Amphiphilic cationic macromolecule potentiates tetracycline against multi-drug resistant Gram-negative bacteria, *Bull. Mater. Sci.*, 2020, **43**, 311.